Conference on Modelling Fluid Flow (CMFF'09)
The 14th International Conference on Fluid Flow Technologies
Budapest, Hungary, September 9-12, 2009

NUMERICAL INVESTIGATION OF STEADY FLOW PAST AN ELLIPTIC CYLINDER AT VARIOUS ASPECT RATIOS

Eric DIDIER[1,2]

[1] Corresponding Author. Departamento de Engenharia Mecânica e Industrial, Faculdade de Ciências e Tecnologia, Universidade Nova de Lisboa, 2829-516 Caparica, Portugal. Tel.: +351 21 294 85 67, Fax: +351 21 294 85 31, E-mail: deric@fct.unl.pt
[2] MARETEC, Instituto Superior Técnico, Technical University of Lisbon, Lisbon, Portugal.

ABSTRACT

The effect of aspect ratio on steady laminar fluid flow past an elliptical cylinder is investigated numerically at two low Reynolds numbers, 20 and 40. The two-dimensional Navier-Stokes equations are solved using an original fully coupled resolution method, without any transformation of continuity equation. The wake's length and maximum width, as well as drag coefficient increase as aspect ratio increases. A pair of steady vortices forms when aspect ratio reaches a critical value.

Keywords: CFD, elliptic cylinder, finite volume, fully coupled resolution method

NOMENCLATURE

AR	[-]	aspect ratio
ARc	[-]	critical aspect ratio
C_D	[-]	drag coefficient
C_{Df}	[-]	viscous drag coefficient
C_{Dp}	[-]	pressure drag coefficient
Cp	[-]	pressure coefficient
Cp_b	[-]	base pressure coefficient
Cp_S	[-]	pressure coefficient at front stagnation point
D	[m]	circular cylinder diameter
La	[m]	major axis
Lb	[m]	minor axis
$Lext$	[m]	computational domain extension
Lw	[m]	recirculation length
Re	[-]	Reynolds number, $U_\infty La/\nu$
S	[-]	non-dimensional cell surface
Sw	[m]	core-stream distance between vortex centres
U_∞	[m/s]	free stream velocity
V	[-]	non-dimensional cell volume
Xw	[m]	vortex centres distance from the rear stagnation point
e	[m]	first grid-point near to the wall
bw	[-]	recirculation width
n	[-]	interface normal vector
p	[-]	non-dimensional pressure
t	[-]	non-dimensional time
u	[-]	non-dimensional velocity
x_i	[-]	non-dimensional Cartesian co-ordinates
ν	[m^2/s]	viscosity
θ	[degree]	angle from the front stagnation point

Subscripts and Superscripts

i	i=1,2	horizontal and vertical directions

1. INTRODUCTION

Cylinders of different cross-sectional shapes, like circular, elliptical and rectangular, are classically used in many engineering applications such as heat exchangers, offshore structures, civil structures and many others. Therefore, due to its large engineering application, the flow past an isolated cylinder has motivated a large number of investigations through theoretical, experimental and computational approaches. In particular, the flow over a circular cylinder has been extensively studied and, consequently, is well documented like is reported by Zdravkovich [1, 2].

In contrast, literature on elliptical cylinders is very limited even though they find application in heat exchangers, airfoils, blades and many others. Characteristic of elliptical cylinder is defined by the aspect ratio AR, ratio of minor axis Lb to major axis La. Several authors have investigated experimentally the flow past elliptical cylinders from moderate to high Reynolds numbers, Re, as Modi and Dikshit [3], Modi et al. [4], Nair and Sengupta [5] and Choi and Lee [6]. Numerically, only limited information is available in unsteady regime and even in the steady regime at low Reynolds numbers. Mittal and Balachandar [7] conducted two- and three-dimensional simulations at Re=525 using a spectral method for an elliptical cylinder with AR=0.5. Johnson et al. [8] studied the effect of AR on low frequency structures in the wake of an elliptical cylinder for Reynolds number in the range of 75 to 175 and by varying the *AR* between a circular cylinder and a flat plate normal to the flow. Sivakumar et al. [9] investigated numerically the flow of power-law fluids across an elliptical cylinder at very low Reynolds numbers, 0.01<*Re*<40. Faruquee et al. [10] presented a study of the effects of aspect ratio on laminar fluid flow at *Re*=40, from an elliptical cylinder, *AR*=0.3, to a circular cylinder, *AR*=1.0, with the major axis parallel to the free-stream. Variation of fundamental quantities and wake parameters versus the *AR* are presented: the wake size and drag coefficient increase with the increase of *AR* and a pair of steady vortices forms when *AR* reaches a critical value. However, the small computational domain size used by Faruquee et al. [10] does not allow grid independent solutions to be obtained. Boubekri and Afrid [11] conducted numerical simulations for an elliptical cylinder with *AR*=0.286 and for Reynolds numbers between 10 and 280 and found three flow regimes.

It can be deduced from the analysis of the existing literature that data on fluid flow over elliptical cylinders is limited, especially at low Reynolds numbers. The role of aspect ratio on flow topology is still not well understood for steady flow. Since measurements become inaccurate at low Reynolds numbers, numerical simulation is a good complement for investigating forces acting on the cylinder and flow topology. However, mesh resolution and computational domain size have to be carefully chosen to reduce numerical errors and to obtain a grid independent solution. Grid independent solution with mesh resolution is routinely carried out. However, fundamental quantities are not only strongly dependent on the mesh resolution but also on the size of the computational domain, as has been demonstrated by Posdziech and Grundmann [12] and Didier [13]. Thus, in order to use numerical simulation in fundamental investigation, a grid independent study has to be carefully realized beforehand to ensure that numerical errors are small as possible.

The present article reports on simulations of two-dimensional steady incompressible laminar flow over an elliptical cylinder, with major axis parallel to the free-stream, for *AR* from 0.2 to 1.0, and for Reynolds numbers *Re*=20 and 40. The longitudinal length *La* is used as the Reynolds number length scale. The effects of aspect ratio are investigated by examining the flow topology, drag coefficient, wake characteristics, base pressure coefficient and pressure coefficient on the cylinder.

2. EQUATIONS

The governing equations for a Newtonian, incompressible viscous flow are the conservation of mass and the Navier-Stokes equations. In dimensionless two-dimensions form and without body forces, they may be written as follows:

$$\frac{\partial u_i}{\partial x_i} = 0 \quad \text{with i=1, 2} \tag{1}$$

$$\frac{\partial u_i}{\partial t} + u_j \frac{\partial u_i}{\partial x_j} = -\frac{\partial p}{\partial x_i} + \frac{1}{Re}\frac{\partial^2 u_i}{\partial x_j^2} \tag{2}$$

where u_i are the non-dimensional velocity components, p is the non-dimensional pressure, *Re* the Reynolds number.

On the circular cylinder surface a no-slip condition is applied, which implies that the fluid velocity is zero.

With the present formulation the velocity field is applied on the external boundary situated far from the cylinder.

$$u_1 = U_\infty \,,\; u_2 = 0 \tag{3}$$

3. NUMERICAL MODEL

3.1. Dimensionless integral equations

The unsteady bidimensional Navier-Stokes equations are written in conservative dimensionless integral form in the referential of the cylinder.

$$\int_S u_j n_j dS = 0 \tag{4}$$

$$\int_V \frac{\partial u_i}{\partial t} dV + \int_S u_i\,(u_j\, n_j) dS = -\int_V \frac{\partial p}{\partial x_i} dV + \frac{1}{Re}\int_S \frac{\partial u_i}{\partial x_j} n_j dS \tag{5}$$

where V is the volume of the element, S is its area and n_i the components of the outward unit vector normal to the surface.

3.2. Fully coupled resolution method

The present numerical code, developed by the author, solves the unsteady, incompressible and two-dimensional Navier-Stokes equations, without any transformation of the continuity equation. In the precedent version of the code, presented by Didier [14] and Didier and Borges [15], a pressure equation has been reconstructed. In the present version of the code, the continuity equation is used in its original form. A finite volume method with collocated cell-centred unknowns is used to discretize the equations for unstructured grids.

Time-dependent solution of these equations requires using an implicit time-integration scheme. Momentum equations are integrated with a three-level second-order scheme. Spatial discretization schemes are implicit too. Diffusion terms are approximated by second-order central-differences scheme. Newton linearization is applied to convective terms. Velocities are approximated by the deferred correction method, using first-order UDS and third-order WACEB [16] schemes for the implicit and explicit part. Pressure at the midpoint face of the control volume is approximated by a second-order linear interpolation. For non-orthogonal grids, corrections are required to estimate velocity components and pressure to the face midpoint of the control volume.

The discretized continuity and momentum equations are gathered in one linear system and solved simultaneously using the iterative algorithm Bi-CGSTAB-ω [17] with an incomplete LU pre-conditioning. The present resolution method does not require any dual-time scheme like in the artificial compressibility or pressure correction methods, or any relaxation parameters.

3.3. Mesh independence results for flow over a circular cylinder

Flow over a circular cylinder at *Re*=40 is simulated. The no-slip condition is applied to the body wall and free-stream velocity condition is imposed on the outer circular boundary. The computational domain extension, *Lext*, is equal to 300*D*, where *D* is the cylinder diameter. Figure 1 shows a schematic view of the computational domain and the position of the outer boundary. Table 1 presents the characteristics of six grids. A grid refinement study is presented Tables 2 and 3 and revealed that an O-grid with N_{ang}=240 and N_{rad}=240 nodes in angular and radial directions respectively, with a first grid-point near to the wall at $e/D=10^{-3}$, is well adapted to the present simulations. The wake's length, *Lw*, drag coefficient, C_D, and pressure base coefficient, Cp_b, obtained with this mesh are within 0.02% of those obtained with a finer grid solution.

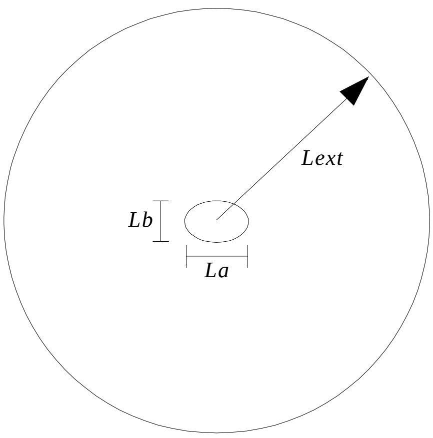

Figure 1. Schematic of the computational domain, cylinder and outer circular boundary

Table 1. Mesh characteristics

Mesh	*e/D*	N_{rad}	N_{ang}	N_{total}
1	0.005	140	120	16800
2	0.001	170	120	20400
3	0.001	170	240	40800
4	0.001	240	120	28800
5	0.001	240	240	57600
6	0.001	295	340	100300

Table 2. Fundamental quantities with grid refinement for a circular cylinder at *Re*=40

Mesh	*Lw/D*	C_D	$-Cp_b$
1	2.18509	1.51645	0.62864
2	2.14310	1.50883	0.62979
3	2.22784	1.50229	0.62249
4	2.14210	1.50913	0.62965
5	2.22594	1.50239	0.62299
6	2.22546	1.50269	0.62307

Table 3. Errors of fundamental quantities with grid refinement for a circular cylinder at *Re*=40

Mesh	E(*Lw*)%	E(C_D) %	E($-Cp_b$)%
1	1.814	0.916	0.894
2	3.701	0.409	1.079
3	0.107	0.027	0.093
4	3.746	0.429	1.056
5	0.022	0.020	0.013
6	0	0	0

Table 4 and 5 show asymptotic convergence of fundamental quantities of flow past a circular cylinder at *Re*=20 for a computational domain size varying from 20*D* to 4800*D*. Numerical results are strongly dependent on the mesh resolution, like it was shown previously in Table 3 and 4, and even more on the size of the computational domain, i.e. the position of the outer boundary. The errors of fundamental quantities, defined using the converged solution obtained for *Lext*/*D*=4800, decrease significantly with increasing size of the computational domain, *Lext*. For small domain extensions, like 20*D*, errors are larger than 1%. When *Lext*=60*D*, wake length error is inferior to 1%. However, drag and base pressure coefficient still exhibit an error around 1.5% and 5% respectively. For *Lext*/*D*=500, errors become inferior to 0.5%. Figures 2 and 3 show the present results and a comparison with results obtained by Posdziech and Grundmann [12] that performed a grid independent solution study using a numerical spectral method. The curves show similar trends. A difference is observed for small computational domain size, due to the type of boundary conditions used in each method, but for domain size larger than 60-80*D*, values of fundamental quantities are very similar. Converged solutions of the two methods present a difference inferior to 0.05%. Results obtained by other authors, like Baranyi and

Lewis [18] using *Lext*=40*D*, Henderson [19] with *Lext*=28*D* and Lange [20] with *Lext*=200*D*, confirm that dispersion of fundamental quantities values, observed in the literature, are related to computational domain extension.

Table 4. Fundamental quantities with computational domain extension at *Re*=20

Lext/La	*Lw/D*	C_D	$-Cp_b$
20	0.91437	2.09496	0.63388
60	0.90955	2.02636	0.56482
140	0.90475	2.00848	0.54646
500	0.90194	2.00031	0.54113
1000	0.90146	1.99717	0.53912
2500	0.90115	1.99487	0.53831
4800	0.90107	1.99394	0.53813

Table 5. Errors of fundamental quantities with computational domain extension at *Re*=20

Lext/La	E(*Lw*)%	E(C_D) %	E($-Cp_b$)%
20	1.48	5.07	17.79
60	0.94	1.63	4.96
140	0.41	0.73	1.55
500	0.10	0.32	0.50
1000	0.04	0.16	0.18
2500	0.01	0.05	0.03
4800	0	0	0

With the present consideration, the circular outer boundary of the computational domain having a radius of 300*D* was chosen to simulate the unbounded flow past a cylinder. Numerical blockage effect is negligible and fundamental quantities errors are inferior to 0.5% for a circular cylinder shape.

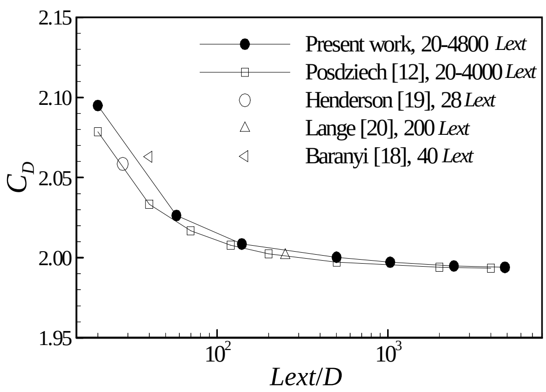

Figure 2. Drag coefficient versus the computational domain extension at *Re*=20

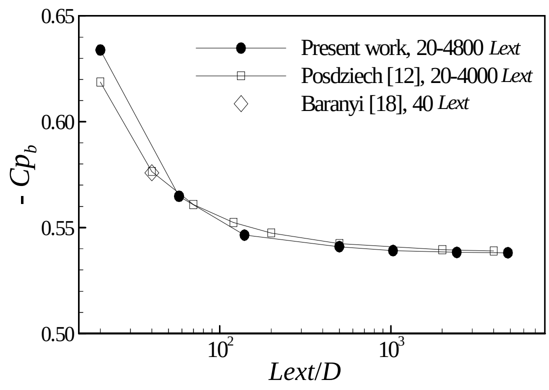

Figure 3. Base pressure coefficient versus the computational domain extension at *Re*=20

4. RESULTS AND DISCUSSION

For *Re*=20 and 40, it is well established that the flow over a circular cylinder is symmetric. A steady state wake forms behind the circular cylinder. The wake length, *Lw*, is defined as the streamwise distance between the wake saddle point (where velocity magnitude is zero) and the stagnation point on the rear of the cylinder.

Numerical simulation predicts a pair of stable, counter-rotating and symmetrical vortices behind the circular cylinder, at *AR*=1.0, in agreement with the existing experimental data. Coutanceau and Bouard [21] experimentally determined the wake length for flow past a circular cylinder for various blockage ratios and extrapolated the wake length for unbounded flow at *Re*=20 and *Re*=40: *Lw*/*La*=0.93 and *Lw*/*La*=2.13. Present results, *Lw*/*La*=0.916 and *LwLa*=2.22, at *Re*=20 and 40 respectively, agree well with these experimental data and with numerical result obtained by Faruquee et al. [10], *Lw*/*La*=2.31 at *Re*=40, and data from the literature.

Numerical simulation predicts a pair of stable, counter-rotating and symmetrical vortices behind the elliptical cylinder. Figure 4 and 5 show the non-dimensional wake length, *Lw*/*La*, and maximum width, *bw*/*La*, versus aspect ratio at *Re*=20 and 40, respectively. Wake length for *Re*=40 is compared with that obtained by Faruquee et al. [10]. Wake length decreases with decreasing *AR*. Below a critical aspect ratio, *ARc*, the standing eddies disappear, as expected since the cylinder becomes more streamlined. *ARc* values are obtained from extrapolation of the numerical data using a polynomial second order fit curve: *ARc*=0.5648 and *Arc*=0.4076, at *Re*=20 and 40, respectively. Faruquee et al. [10] found a different value of critical aspect ratio at *Re*=40, *ARc*=0.34, certainly due to the smaller computational domain used in their simulations.

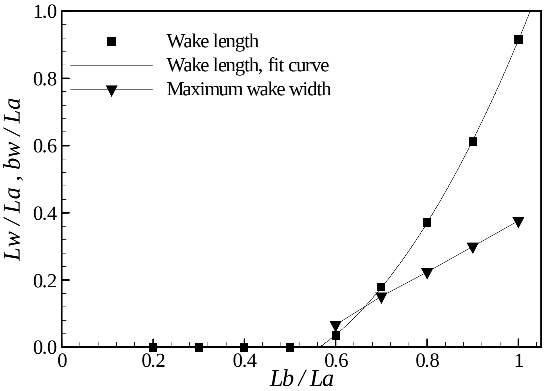

Figure 4. Effect of *AR* on the wake length and width at *Re*=20

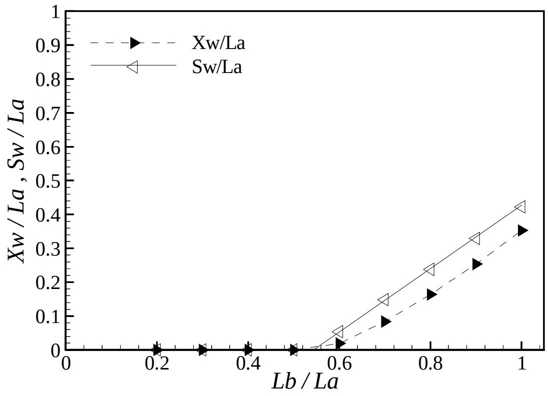

Figure 6. Effect of *AR* on the vortex centre positions at *Re*=20

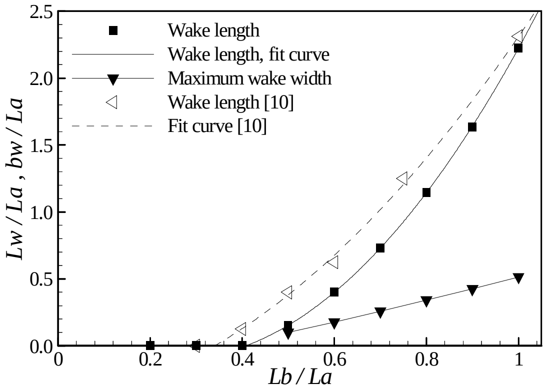

Figure 5. Effect of *AR* on the wake length and width at *Re*=40

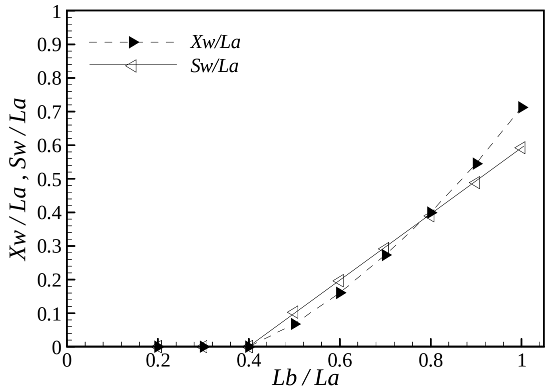

Figure 7. Effect of *AR* on the vortex centre positions at *Re*=20

Maximum wake width varies linearly with *AR*. When separation of the boundary layer occurs, at *ARc*, the maximum width is situated at the separation point. As *AR* is increased the maximum width location moves downstream from the separation point and *bw* increases (see also Figures 10 to 13).

Figures 6 and 7 show the position of the centres of eddies, *Xw*, and the core-stream distance between vortex centres, *Sw*, respectively. Wake cores, i.e. vortex centres, are defined in terms of their x_1 coordinate as the distance from the rear stagnation point of the cylinder, and x_2 coordinate as the distance from the rear axis. Coutanceau and Bouard [21] measured the distances of the vortex centres from the circular cylinder rear stagnation point and from the near wake axis (streamwise rear axis). In present simulation, at *Re*=40, the centres of the vortices formed behind the circular cylinder were found at a streamwise distance of 0.71*La* from the rear stagnation point and at a cross-stream distance of ±0.295*La* from the wake axis. These are in very good agreement with the findings of Coutanceau and Bouard [21] for an unbounded cylinder, who estimated the distances as 0.76*La* from the rear stagnation point and ± 0.295*La* from the wake axis, respectively. From Figures 6 and 7, it is show that distance between the vortex centres, *Sw*, increases linearly with *AR*, for *Re*=20 and *Re*=40. The variation of distance of the vortex centres from the rear stagnation point, *Xw*, with *AR* is not linear, for both Reynolds numbers. These behaviours are not observed by Faruquee et al. [10], since they found that *Sw* is to be approximately quadratically related with *AR*, and that *Xw* varies linearly. The discrepancy observed between the present results and Faruquee et al. [10] results can be due to the small domain used by these authors.

Figures 8 and 9 show total drag, C_D, viscous drag, C_{Df}, and pressure drag, C_{Dp}, coefficients versus *AR* for *Re*=20 and 40, respectively. Present results are compared those obtained by Sivakumar et al. [9] and Faruquee et al. [10]. The drag coefficient increases with the increase of *AR* and is maximum for a circular cylinder. The viscous drag coefficient is found to decrease at a small rate whereas the pressure drag coefficient increases rather sharply with increasing *AR*. Fit curves allow to confirm that pressure drag is zero for *AR*=0, a thin flat plate, and that viscous drag is the sole contributor to drag coefficient. Extrapolated values

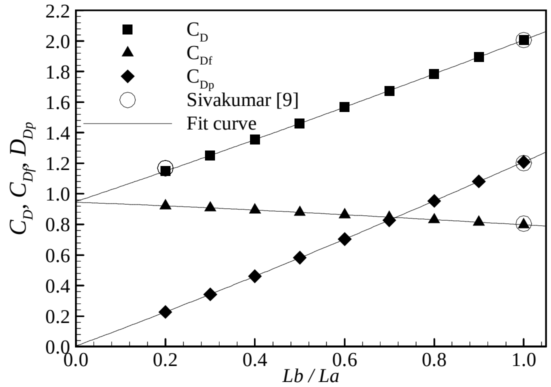

Figure 8. Drag coefficient, C_D, C_{Df} and C_{Dp} versus *AR* at *Re*=20

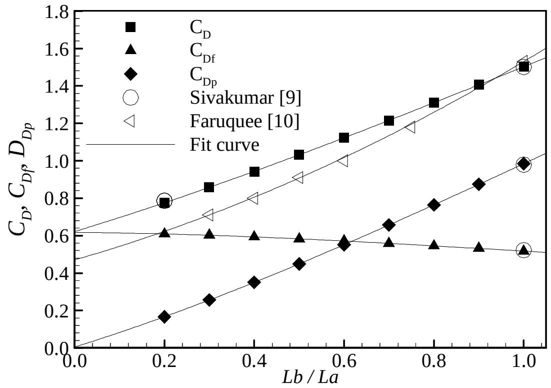

Figure 9. Drag coefficient, C_D, C_{Df} and C_{Dp} versus *AR* at *Re*=40

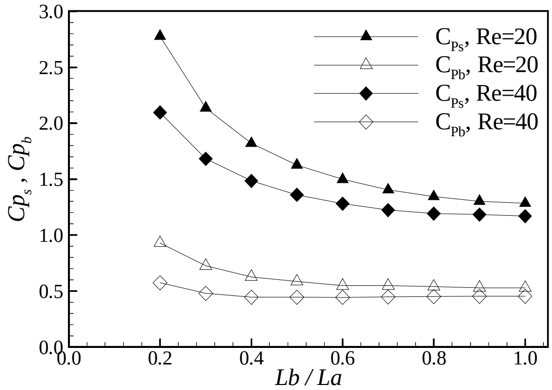

Figure 10. Cp at front stagnation point and *Cpb* versus *AR*, at *Re*=20 and 40

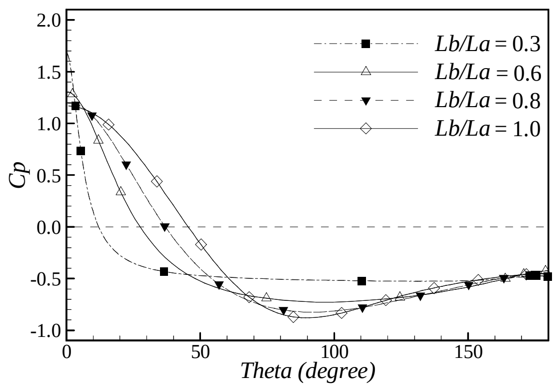

Figure 11. Effect of *AR* on the *Cp* on the elliptical cylinder, at *Re*=40

of viscous drag are 0.945 and 0.617 for *Re*=20 and 40, respectively.

Present results agree very well with that obtained by Sivakumar et al. [9] for a circular cylinder and an elliptical cylinder with *AR*=0.2. The authors in their numerical simulations used a large computational domain with 300*La*. However, drag coefficient found by Faruquee et al. [10] is not in accordance with these results. Faruquee et al. [10] use a very fine grid, but the computational domain size is too small, with an outer radius of circular boundary of just 40*La*. Fundamental quantities are strongly dependent not only of the mesh refinement but also of the computational domain size. This explains the discrepancy of Faruquee's results.

Figure 10 shows the pressure coefficient on the front stagnation point, Cp_S, and the base pressure coefficient on the rear stagnation point, Cp_b, versus *AR* at *Re*=20 and 40. Pressure coefficient is defined using the reference pressure at the inlet boundary. As can be expected at low Reynolds numbers flows, pressure coefficient on front and rear stagnation points decrease when *Re* increases. Pressure coefficient on front stagnation point also decreases with the increase of *AR*. However, base pressure coefficient decreases only until the *ARc*. For *AR*>*ARc* base pressure coefficient is quasi constant and is not significantly dependent on the *AR* or wake characteristics.

Figure 11 shows the pressure coefficient on the cylinder at *Re*=40, from the leading edge, θ=0°, to the trailing edge, θ=180°, for *AR*=0.3, 0.6, 0.8 and 1.0. The *AR* influences strongly the pressure coefficient. The pressure drop becomes sharper at the cylinder front as *AR* decreases and *Cp* at the front stagnation point increases. *Cp* is constant along the cylinder for *AR*=0.3, before the *ARc*. When flow separation occurs *Cp* presents a minimum value. For a circular cylinder the minimum *Cp* occurs at 89.3°. As the *AR* decreases the minimum *Cp* value increases and take place at angular position greater than 89.3°: 91.4° for *AR*=0.8 and 96.8° at *AR*=0.6.

Figure 12 to 15 show the streamlines over a cylinder for *AR*=0.3, 0.6, 0.8 and 1.0, respectively, at *Re*=40. The flow is symmetrical. Symmetrical counter rotating vortices are observed behind the cylinder for *AR*>*ARc*. The wake length and maximum width increase with *AR*, as it was demonstrated before.

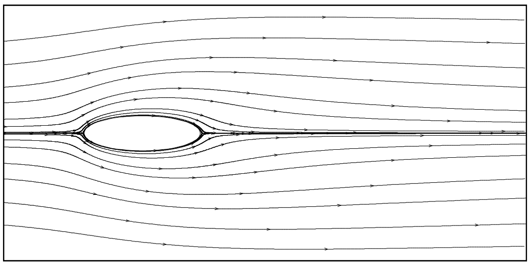

Figure 12. Flow topology at *Re*=40 at *AR*=0.3

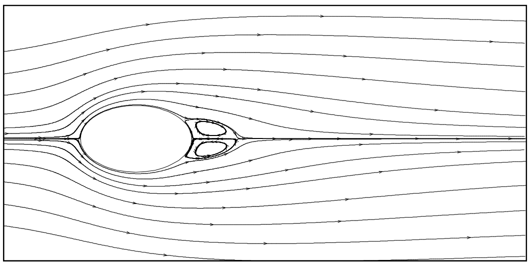

Figure 13. Flow topology at *Re*=40 at *AR*=0.6

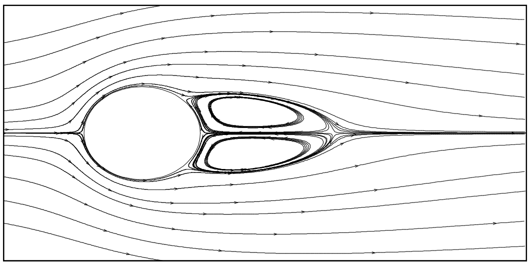

Figure 14. Flow topology at *Re*=40 at *AR*=0.8

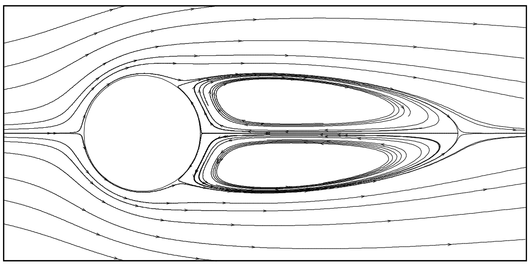

Figure 15. Flow topology at *Re*=40 at *AR*=1.0

5. CONCLUSIONS

Fluid flow around an elliptical cylinder is numerically investigated, at Reynolds number 20 and 40, to access the effects of aspect ratio from 0.2, a streamlined elliptical cylinder, to 1.0, a circular cylinder.

The study also addresses the effect of computational domain size and mesh refinement on fundamental quantities for a circular cylinder. Present results agree well with a similar study realized using a spectral method. Both works show that fundamental quantities are strongly dependent not only of the mesh refinement but also of the computational domain size.

The present study of flow past an elliptic cylinder of different aspect ratio shows that

- No vortices exist behind the cylinder for *AR*<*ARc*.
- Critical *ARc*, for that vortices to appear behind the cylinder, are determined as *ARc*=0.5648 and *ARc*=0.4076 for *Re*=20 and 40, respectively.
- Wake width, wake length, C_D and C_{Dp} increase as *AR* increases while C_{Df} decreases slowly.
- Distance between the vortex centres, *Sw*, increases linearly with *AR*, for both Reynolds numbers. The variation of distance of the vortex centres from the rear stagnation point, *Xw*, with *AR* is not linear.
- Pressure coefficient on front stagnation point decreases with the increase of *AR*.
- However, base pressure coefficient decreases only until the *ARc*. For *AR*>*ARc* base pressure coefficient is quasi constant and is not significantly dependent on *AR*.

Future study on unsteady flow over an elliptic cylinder with different axes ratio and Reynolds number is planed.

REFERENCES

[1] Zravkovich, M.M., 1997, *Flow around circular cylinders, Fundamentals*, vol.1, Oxford University Press Inc., New York, USA.

[2] Zravkovich, M.M., 2003, *Flow around circular cylinders, Applications*, vol.2, Oxford University Press, Oxford.

[3] Modi, V.J., and Dikshit, A.K., 1975, “Near-wakes of elliptic cylinders in subcritical flow”, *AIAA J.*, Vol. 13, pp. 490-497.

[4] Modi, V.J., Wiland, E. , Dikshit, A.K., and Yokomizo, T. , 1992, “On the fluid dynamics of elliptic cylinders”, *Int. J. Offshore Polar Eng*, Vol. 2, pp. 267-280.

[5] Nair, M.T., and Sengupta, T.K., 1996, “Onset of asymmetry: flow past circular and elliptic cylinders”, *Int. J. Numer. Methods Fluids*, Vol. 23, pp. 1327-1345.

[6] Choi, J.H., and Lee, S.J., 2001, “Flow characteristics around an inclined elliptic cylinder in a turbulent boundary layer”, *Journal of Fluids and Structures*, Vol. 15, pp. 1123-1135.

[7] Mittal, R., and Balachandar, S., 1996, “Direct numerical simulation of flow past elliptic

cylinders", *J. Comput. Phys.*, Vol. 124, pp. 351-367.

[8] Johnson, S.A., Thompson, M.C., and Hourigan, K., 2004, Predicted low frequency structures in the wake of elliptical cylinders, *European Journal of Mechanics B/Fluids*, Vol. 23, pp. 229-239.

[9] Sivakumar, P., Prakash Bharti, R., and Chhabra, R.P., 2007, "Steady flow of power-law fluids across an unconfined elliptical cylinder", *Chemical Engineering Science*, Vol. 62, pp. 1682-1702.

[10] Faruquee, Z., Ting, D.S-K., Fartaj, A., Barron, R.M., and Carriveau, R., 2007, "The effects of axis ratio on laminar fluid flow around an elliptical cylinder", *International Journal of Heat and Fluid Flow*, Vol. 28, pp. 1178-1189.

[11] Boubekri, M. and Afrid, M., 2008, "Some Modes of the incompressible flow on an elliptic cylinder at low Reynolds number", *Journal of Engineering and Applied Sciences*, Vol. 3(1), pp. 94-99.

[12] Posdziech, O., and Grundmann, R., 2007, "A systematic approach to the numerical calculation of fundamental quantities of the two-dimensional flow over a circular cylinder", *Journal of Fluid and Structures*, Vol. 23, pp. 479-499.

[13] Didier, E., 2008, "Convergência assimptótica das quantidades fundamentais na modelação numérica do escoamento em torno de um cilindro circular", Proc. *II Conferência Nacional de Métodos Numéricos em Mecânica de Fluidos e Termodinâmica*, Aveiro, Portugal. (in Portuguese)

[14] Didier, E., and Borges, A.R.J., 2007, "Numerical predictions of low Reynolds number flow over an oscillating circular cylinder", *Journal of Computational and Applied Mechanics*, Vol. 8:1, pp. 39-55.

[15] Didier, E., 2007, "Flow simulation over two circular cylinders in tandem", *C.R. Mécanique*, Vol. 335, pp. 696-701.

[16] Song, B., Liu, G.R., Lam, K.Y., and Amano, R.S., 2000, "On a higher-order bounded discretization scheme", *Int. J. Numer. Meth. Fluids*, Vol. 32, pp. 881-897.

[17] Sleijpen, G.L.G., and van der Vorst, H.A., 1995, "Maintaining convergence properties of BiCGSTAB methods in finite precision arithmetic", *Numer. Algorithms*, pp. 203-223.

[18] Baranyi, L., and Lewis, R.I., 2006, "Comparison of grid-based and vortex dynamics predictions of low Reynolds number cylinder flows", *Aeronaut. J.*, Vol. 110, pp. 63-71.

[19] Henderson, R.D., 1995, "Details of the drag curve near the onset of vortex shedding", *Physics of Fluids*, Vol. 7, pp. 2102-2114.

[20] Lange, C., 1997, "Numerical predictions of heat and momentum transfer from a cylinder in crossflow with implications to hot-wire anemometry", *Phd Thesis, University Erlangen-Nürnberg*.

[21] Coutanceau, M., and Bouard, R., 1977, "Experimental determination of the main features of the viscous flow in the wake of a circular cylinder in uniform translation, part 1. Steady Flow", *Journal of Fluids Mechanics*, Vol. 79, pp. 231-256.